Chapter 5

Migration-assisted energy transfer at polymer/metal interfaces

Summary

The dynamics of exciton quenching in a conjugated polymer due to the presence of metal films is analyzed using time-resolved photoluminescence. The quenching is governed by direct radiationless energy transfer to the metal and is further enhanced by diffusion of excitons into the depletion area of the exciton population at the polymer/metal interface. The time-resolved luminescence is described by a numerical exciton diffusion model with the energy transfer incorporated via long-range dipole-dipole interaction at the metallic mirror. This allows us to disentangle the contributions from direct energy transfer to the metal and exciton migration to the exciton quenching process. For an aluminum electrode strong exciton quenching occurs in a region of typically 15 nm, which can be decomposed in a characteristic energy transfer range of 7.5 nm and an exciton diffusion length of 6 nm.

5.1 Introduction

In PLEDs [1,2] metallic electrodes are used to inject charge carriers that subsequently form excitons. However, the presence of a metallic film allows excitons to transfer their energy nonradiatively towards the electrode, thereby lowering the efficiency of the PLED [3]. Also in photovoltaic devices [4, 5] excitons formed upon photoexcitation can transfer their energy to the metallic electrodes, thereby reducing the yield of free charge-carrier production [6]. The effect of metal films on the photoluminescence (PL) and electroluminescence (EL) of conjugated polymers has been extensively studied using time-integrated PL [3]. From the dependence of the PL quantum yield on the thickness of the polymer film a typical width of the exciton quenching region can be estimated. For cyanoderivatives of poly(*p*-phenylene vinylene) (PPV) it has been demonstrated that both PL and EL of the polymer are strongly quenched within a typical distance of 20 nm from gold or aluminum interfaces [3]. The obtained characteristic quenching distance with respect to the metal interface can then be used as a measure for the effectiveness of the exciton quenching process. However, it does not discriminate between various mechanisms that contribute to the quenching process. In fact, there are two main processes that are responsible for exciton quenching by metallic films.

The first is the nonradiative energy transfer from the excited polymer to the metal via long-range dipole-dipole interaction. This process provides an extra exciton decay channel and results in an enhancement of the nonradiative decay rate close to the metal. The radiative (intrinsic) properties of the emissive species are also modified by the metal mirror due to interference effects. This has been demonstrated to be important for highly luminescent conjugated polymers [3]; radiative exciton lifetime modification increases with increasing luminescence quantum efficiency of the material and becomes distinct at long distances from the metal interface [7, 8]. A detailed theory of an oscillating dipole and energy transfer near metal interfaces has been developed [9, 10] and agreement between experiment and theory has been demonstrated by Chance and co-workers [7,11]. It should be noted that for calculating the lifetime (or quantum efficiency) of the luminescence of a conjugated polymer near a metal interface additional assumptions about the dipole orientation and intrinsic quantum efficiency need to be made.

The second process is the migration of the excitation energy inside the conjugated polymer. The occurrence of nonradiative energy transfer to the the metal will lead to a gradient in the exciton population close to the metallic film. As a result, excitons will diffuse towards the metal interface, which increases the overall efficiency of the exciton quenching process. The exciton diffusion length in conjugated polymers, typically 5-10 nm [12, 13], is of the same order of magnitude as the estimates for the range of energy transfer to the metal. Therefore, a fundamental question to be solved is which of these two processes is mainly responsible for the quenching of excitons at metallic interfaces. In order to disentangle these two contributions, knowledge about the exciton migration dynamics, characterized by the exciton diffusion coefficient, is required. So far, the study of exciton diffusion in conjugated polymers has mainly been focused on the extraction of the exciton diffusion length L_D. In a recent study,

we were able to extract both exciton diffusion coefficients and diffusion lengths from time-resolved PL measurements on a bilayer model system, consisting of PPV-based conjugated polymers and a polymerized fullerene [12, 14, 15]. In this chapter we analyze the dynamics of the quenching of excitons at metal interfaces by monitoring the time-resolved luminescence of a PPV-based conjugated polymer. Our knowledge of the exciton migration in the neat polymer enables us to disentangle the contributions from both the exciton diffusion and energy transfer to the metal, to the exciton quenching process.

5.2 Excitons at metal interfaces

An extensive physics literature on the effects of luminescence modification due to the presence of metals exists. In this section we provide a selected summary of those results that concern performance of polymer optoelectronic devices.

A competition between radiative and nonradiative excitonic processes in conjugated polymer light-emitting diodes as well as in photovoltaics governs the device efficiency. Most of optoelectronic devices contain metallic films used as charge injection or collection electrodes, or mirrors for light out-coupling or concentration. The presence of a metal film will always influence the properties of the emitting material. Microcavities have been used to narrow the linewidth and tune the emission color from conjugated polymers [16]. It has been also shown that spontaneous emission rate of fluorophores [17], and conjugated polymers in particular [18], can be greatly enhanced or suppressed by the use of metal islands, metal colloids, metal surfaces, or mirrors.

Generally, the luminescence lifetime τ is related to the rate constants for radiative (k_r) and nonradiative (k_{nr}) decay by

$$\frac{1}{\tau} = k_r + k_{nr}, \tag{5.1}$$

where the radiative lifetime is $1/k_r$. The quantum efficiency for luminescence q_r is given by

$$q_r = b\Big(\frac{k_r}{k_r + k_{nr}}\Big), \tag{5.2}$$

where the branching ratio b is the fraction of absorbed photons leading to singlet excitons. The balance between the radiative and the nonradiative decay rates therefore determines the luminescence efficiency. At that, the presence of a metallic interface opens up additional nonradiative (k_{nr}) exciton loss channels and alters radiative (k_r) 'intrinsic' properties of the polymer phase of the device.

The effect of metal films on PL and EL of conjugated polymers has been extensively studied; and experimental data of luminescence quantum efficiency for polymer films of varying thickness in front of metal layers, have been reported to characterize the overall exciton quenching process [3]. In this study Becker and co-workers have demonstrated that both PL and EL of cyano- derivatives of poly(p-phenylene vinylene) (PPV) are strongly quenched within a typical distance of 20 nm from gold

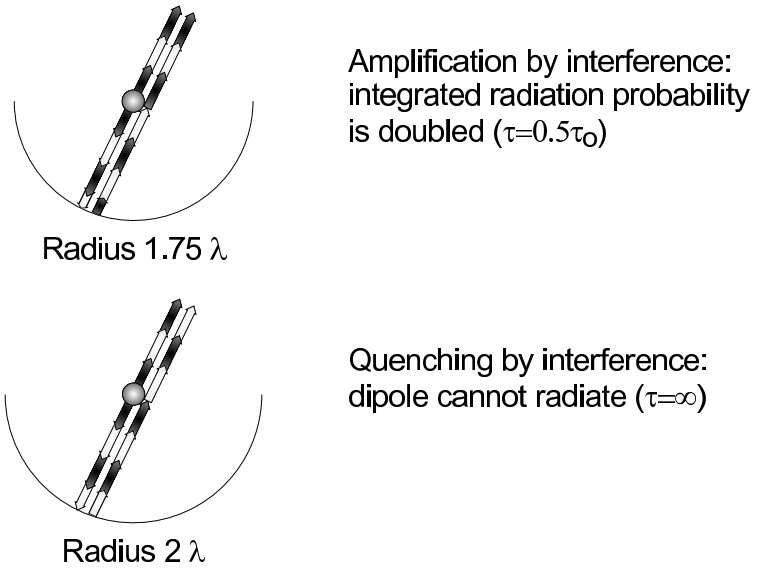

Figure 5.1: Radiation from excited molecule in the center of spherical mirror [19].

or aluminum interfaces. A complete theoretical description of exciton quenching in polymer films at metal interfaces requires an understanding and characterization of the whole set of relevant excitonic processes. Besides thermally activated exciton diffusion, which shifts a part of the exciton population toward the quenching well at the metallic interface, there are effects of the metal mirror, that alter both radiative (k_r) and nonradiative (k_{nr}) decay rates.

5.2.1 Interference effects

To demonstrate modification of the radiative decay rates let us consider the radiation of an oscillating electric dipole (an excited molecule) in the very center of a spherical mirror(Fig. 5.1).If the radius of the mirror is for instance 1.75λ (Fig. 5.1, upper case), constructive interference of the direct and reflected wave will occur in all directions of the upper half-space. Since the radiated intensity is proportional to the square of the amplitude, the probability for radiation is four times as large as without the mirror. Into the lower half space there is no radiation due to the mirror. Therefore the integrated probability for radiation will be twice as large as without the mirror. This means the decay time of the molecule in the center of the mirror will be half the decay time of the molecule in free space (assuming there are no competing nonradiative deactivation processes). On the other hand, if the radius of the spherical mirror is for instance 2λ (Fig. 5.1, lower case), the direct and reflected beam interfere destructively and thus the excited molecule cannot radiate at all (decay time infinite).

In the same way as shown for a spherical mirror the fluorescence decay time is

affected by a plane mirror. Analytical form of the decay time τ dependence on distance d from the mirror has been derived by Drexhage and coworkers by integration of the intensity above the mirror [8, 20]:

- axis of electric dipole oscillator perpendicular to the mirror

$$\frac{\tau_\perp}{\tau_\infty} = \left[1 - \frac{3}{2}\int_0^1 \rho_\parallel(u)(1-u^2)\cos(xu - \delta_\parallel(u))du\right]^{-1}; \tag{5.3}$$

- axis of electric dipole oscillator parallel to the mirror

$$\frac{\tau_\parallel}{\tau_\infty} = \left[1 + \frac{3}{4}\int_0^1 \left[\rho_\perp(u)\cos(xu - \delta_\perp(u)) + \rho_\parallel(u)u^2\cos(xu - \delta_\parallel(u))\right]du\right]^{-1}, \tag{5.4}$$

where $x = 4\pi nd/\lambda$; u is a cosine of the incidence angle; $\rho_\parallel, \rho_\perp$ - reflection coefficients of the mirror, $\delta_\parallel, \delta_\perp$ - phase shifts on reflection by the mirror.

The decay times for electric dipoles parallel and perpendicular to a golden mirror are simulated and shown in Fig. 5.2a for the idealized case (no nonradiative processes). If transition dipole moment does not have any preferred orientation, the expected decay time τ_a (Fig. 5.2a, solid curve) is given by the average

$$\frac{1}{\tau_a} = \frac{2}{3}\frac{1}{\tau_\parallel} + \frac{1}{3}\frac{1}{\tau_\perp}. \tag{5.5}$$

A decrease in the lifetime is found when the reflected field is in-phase with the fluorophore's oscillating dipole; and an increase in the lifetime is observed if the reflected field is out-of-phase with the oscilating dipole. The amplitude of the decay time oscillations reduces with distance from the mirror; at large distances $\tau \to \tau_\infty$.

In the above considerations, possible radiationless deactivation processes, which are not affected by the mirror, were omitted. The quantum yield of the emitting state q must be known for simulation of the true decay time. The anisotropy of the dipole moment orientations is another important issue that should be taken into account. For instance, fabrication of the polymer films by spin-coating implies preferential orientation of the dipole moments parallel to the interface. Simulation of the decay time for $q = 0.3$ and $\eta = 90$ % of the dipoles oriented in-plane is shown in Fig. 5.2b. A quantum yield $q < 1$ leads to a less pronounced variation of the fluorescence decay time in front of the mirror, because in this case the radiationless deactivation processes which are not affected by the mirror, have an influence on the decay time.

The possibility of altering the radiative decay rates was demonstrated by Drexhage in 1966 by measurements of the decay times of europium (Eu^{3+}) complex positioned at various distances from a planar silver mirror [20]. Fatty acid layers were deposited by Langmuir-Blodgett technique to separate a fluorescent dye from the metal interface. The lifetime oscillate with distance but remain a single exponential at each distance (Fig. 143). This effect can be again explained by changes in the phase of the reflected field with distance and the effects of this reflected field on the fluorophore. The interference theory presented above has been used to model these experimental data

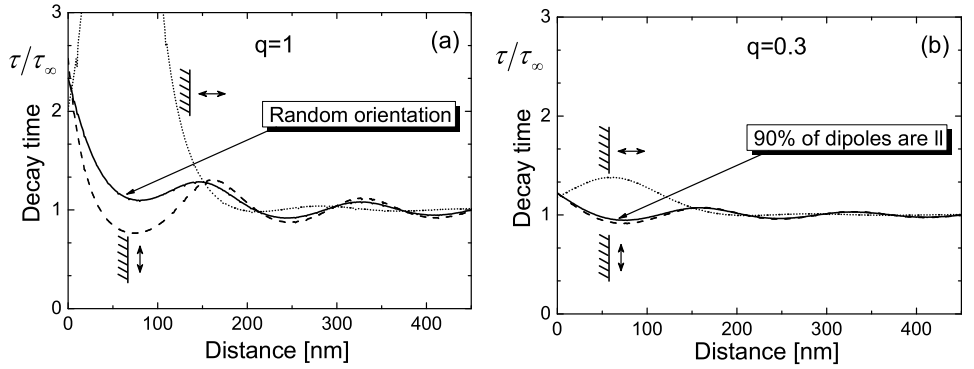

Figure 5.2: Decay time of the dipole oscillator in front of a gold mirror. $q = 1$ and $\eta = 67$ %(random) (a); $q = 0.3$ and $\eta = 90$ %.

and a fit with quantum yield $q = 0.7$ (Fig. 5.3, dash curve) has demonstrated a good agreement with experiment [19]. The effects of a plane mirror occur over distances comparable to the excitation and emission wavelengths. The disagreement at short distances is due to the energy transfer from the excited molecules to the silver layer, which is responsible for a strong exciton quenching at very metal interfaces and is of the high importance for device performance.

5.2.2 Energy transfer

The effect of a metal film on the lifetime of an excited molecule has been elegantly determined by Chance and coworkers by the use of the energy flux method where the total energy flux through infinite planes above and below the dipole is calculated [7]. It gives separate expressions for the effects of interference on the radiative decay rate and of nonradiative energy transfer on the nonradiative decay.

The nature of the nonradiative anergy transfer depends on the distance of the oscillating dipole to the metal. In the broad distance range the interaction of the dipole with the electron gas of the metal is dominated by the bulk effects (electron-phonon or electron-impurity scattering). This implies an inverse cubic distance x dependence of the transfer rate

$$r_{me} = \frac{1}{\tau_\infty} \frac{{x_0}^3}{x^3}, \tag{5.6}$$

where τ_∞ is the intrinsic exciton lifetime, and x_0 is the characteristic distance of the energy transfer [7, 9]. Eq. 5.6 has been experimentally demonstrated to hold for distances down to 3 nm [28]. This study the quenching of anthracene fluorescence by the thick aluminum contact has been monitored, while varying the fluorophore-metal separation distance by applying different number of fatty acid monolayers. Similar experiments on phosphorescence in pyrazine/physisorbed Ar/nickel structures showed the same distance dependence for spacer thicknesses down to 8 Å [23].

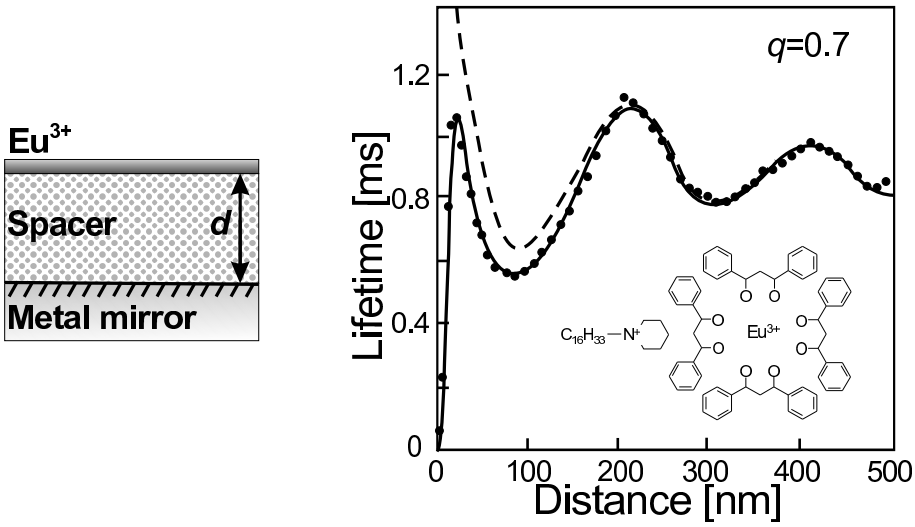

Figure 5.3: Lifetime of Eu^{3+} ions in front of a silver mirror as a function of separation between the Eu^{3+} ions and the mirror. Experimental data (•) are those of Drexhage [19, 20]. Dash curve is a theoretical fit with Eq. 5.5 assuming $q = 0.7$. The solid curve also shows energy transfer effect taken into account [21].

An analytical expression for the transfer range x_0 has been derived in Ref. [7] by Chance and co-workers

$$x_0{}^3 = \frac{3}{32}\frac{\lambda^3\Theta}{\pi^3 n_1}\frac{n_2 K_2}{(n_1{}^2 + n_2{}^2 - K_2{}^2)^2 + 4n_2{}^2K_2{}^2}. \tag{5.7}$$

Here λ is the resonant wavelength, and Θ is a geometric factor varying with orientation of the molecule with respect to the metal (1 for a horizontal dipole, 2 for a vertical one, and 4/3 for randomly oriented dipoles). n_1 is the refractive index of the media, while $n_2 + iK_2$ represents the complex refractive index of the metal with the imaginary part responsible for energy absorption.

At short distances scattering by the surface must be accounted for to consider momentum conservation of metal electrons. A theory developed by Persson and co-workers has predicted an additional $1/x^4$ term to the Eq. 5.6 [10, 24]. Considerable input of this component into the transfer rate distance dependence has been experimentally demonstrated by rhodamine 6G fluorescence lifetime modification at thick aluminum layers with spacer thickness variation up to 6 nm [29].

Chance an co-workers [21] have demonstrated that luminescence lifetime measurements performed by Drexhage for Eu^{3+} complex at silver interface can be accurately modelled by taking both nonradiative energy transfer and interference effects into account (Fig. 5.3, solid curve).

Metal films of finite thickness. Polymer-based optoelectronic devices, like tandem

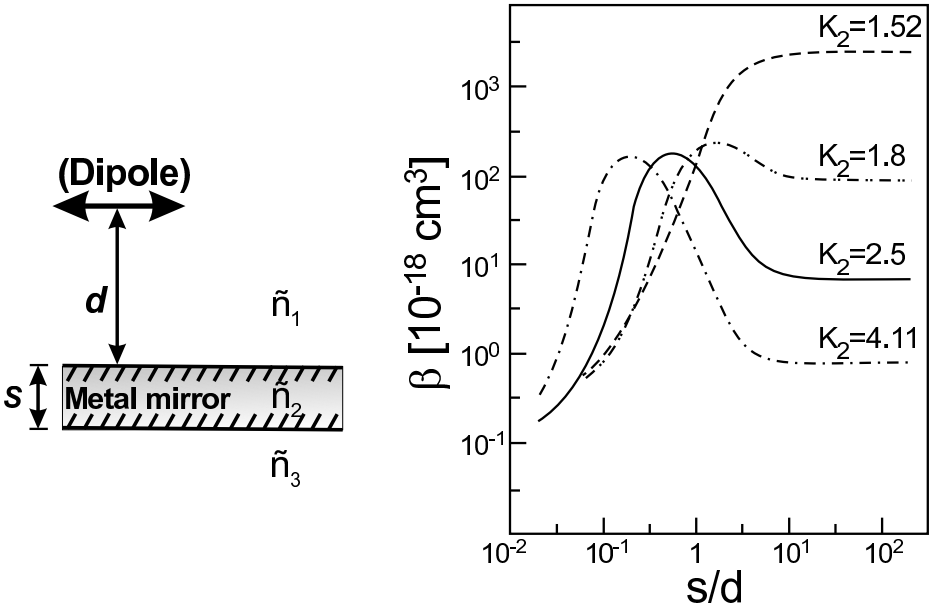

Figure 5.4: The effect of metal mirror thickness on the energy transfer rate parameter β; s is a mirror thickness, d is a dipole-mirror separation, and K_2 is the imaginary part of the refractive index of metal [7]. In all cases $n_1 = n_3 = 1.52$ and $n_2 = 0.06$. Geometry of the dipole-thin metal mirror system is shown on the left.

photovoltaic cells, use semitransparent films of evaporated metals [!Afshin]. Thus the effect of the finite metal film thickness on the energy transfer rate and on the emitter lifetime becomes important. Simulation of the energy transfer rate has been performed by Chance and co-workers with the use of the energy flux method for the range of values of the metal complex refractive index $\tilde{n}_2$ [7]. Results are presented in the form of energy transfer parameter β ($\beta \equiv {x_0}^3$ for an infinite metal film), which now shows dependence on the mirror thickness s to the dipole-mirror separation d ratio (Fig. 5.4). The real part of $\tilde{n}_2$ is selected as 0.06 and the imaginary part covers a span from the value 4.11 (silver film) to the value of 1.52 (matching condition for Eq. 5.7). The monotonically decreasing curve (with decreasing s/d) which describes the matching condition is seen to develop a peak as K_2 moves away from the matching condition. This peak in the case of silver film ($K_2 = 4.11$) is seen to be quite high, rising more then two orders of magnitude over the value for a thick film. The latter analysis clearly demonstrates that the energy transfer efficiency can be dramatically enhanced by the use of finite (very thin) metal films. So, considerable increase of the characteristic energy transfer distance x_0 is expected at semitransparent metal contacts.

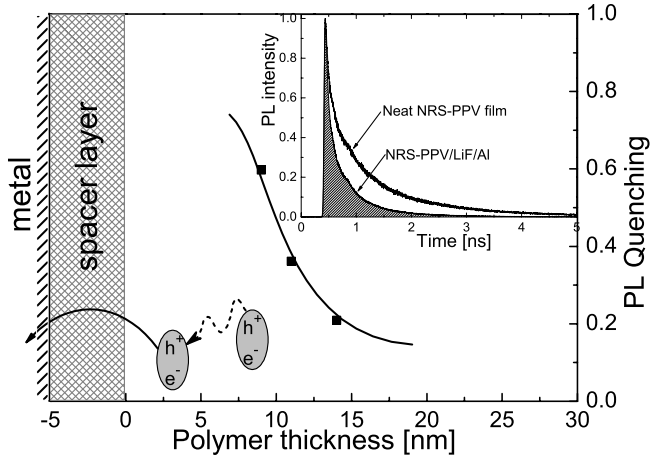

Figure 5.5: PL quenching (■, right axis) in NRS-PPV/LiF/Al structures vs polymer film thickness; the solid line is a guide to the eye. The relative quenching was derived by integration of the PL decay curves (inset). In the schematic diagram of the sample configuration exciton quenching is represented as a combination of diffusion and energy transfer to the metal.

5.3 Energy transfer disentanglement

In order to construct polymer/spacer layer/metal heterostructures (Fig. 5.5), poly[2-(4-(3′,7′-dimethyloctyloxyphenyl))-co-2-methoxy-5-(3′,7′-dimethyloctyloxy)-1,4-phenylene vinylene] (NRS-PPV) was spin coated from a toluene solution on top of the glass substrate under nitrogen atmosphere. Subsequently, thin transparent spacer layers of LiF were thermally evaporated on top of the polymer films and served as exciton blocking layers [26]. Finally, gold or aluminum layers were thermally evaporated on top of the spacer layers. Variation of the spacer layer thickness was employed to investigate the distance dependence of the nonradiative energy-transfer rate.

First, time-resolved PL measurements were performed on NRS-PPV/LiF/aluminum heterostructures. LiF/Al films are widely used as cathodes in polymer photovoltaic cells and light-emitting diodes. The use of a LiF spacer layer has the advantage in that it prevents diffusion of metal atoms into the polymer layer. A LiF layer of 5 nm and 100 nm of aluminum were thermally evaporated on top of NRS-PPV films with varying thicknesses. As a first step a comparison of the (time-integrated) areas under the PL decay curves for structures with and without metal interfaces provides a simple empirical measure for the efficiency of the PL quenching by the metal. As demonstrated before [3], the dependence of the time-integrated PL on polymer thickness then provides a direct estimate of the width of the quenching zone at the polymer/metal interface. In Fig. 1 the relative time-integrated PL quenching [12] is plotted for various NRS-PPV film thicknesses. It appears that strong exciton quench-

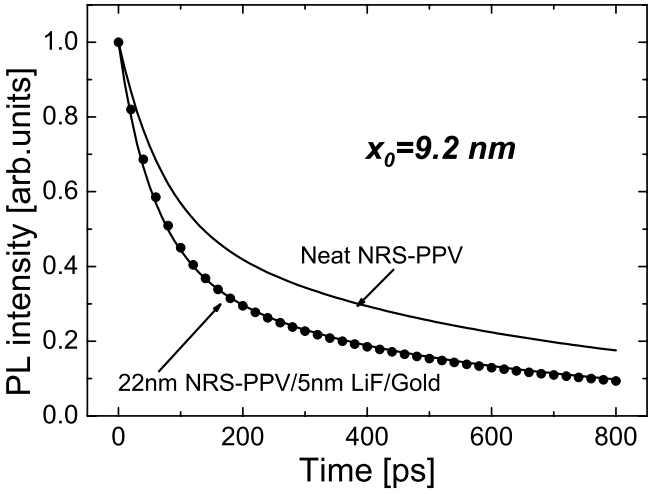

Figure 5.6: Normalized luminescence decay curves for both the NRS-PPV/LiF/gold structure (•)and neat NRS-PPV as a reference (solid line). Simulation of these data by Eq. (3) with transfer range x_0 as a fit parameter.

ing is observed within typically 15 nm from the Al/LiF interface. Note that this width is representative for the total exciton quenching process. As a next step we also investigated NRS-PPV/LiF/gold heterostructures; they are known to be chemically stable model systems with an efficient energy transfer. A normalized and deconvoluted luminescence decay curve of a 22 nm conjugated polymer film is depicted in Fig. 5.6, together with the reference luminescence decay curve of the neat polymer film. Upon the photoexcitation of the polymer excitons are formed. Their migration and nonradiative energy transfer to the metal result in a faster decay of the polymer luminescence. The LiF layer serves as a dielectric spacer and blocks excitons [26, 27], which allows study of the exciton quenching as a function of distance from the metal interface.

The exciton migration process is characterized by the exciton diffusion constant D and the exciton diffusion length L_D, which are related by

$$L_D = \sqrt{D\tau_\infty}, \tag{5.8}$$

where τ_∞ is the exciton lifetime that accounts for the total process of radiative and nonradiative exciton decay. In a recent study an exciton diffusion coefficient of 3×10^{-4} cm^2/s for NRS-PPV has been deduced [14].

The distance (x) dependence of the nonradiative decay rate constant r_{me} for organics in front of metal interfaces has been studied both experimentally [28, 29] and theoreticaly [7], where a general expression has been derived within classical light reflection theory. For the case of interest, corresponding to a small distance between emissive molecule and metal in comparison with the resonant wavelength, it can be

approximated with a x^{-3} dependence (Eq. (5.6)) [7,30].

In order to model the time-resolved luminescence quenching in polymer/spacer/metal heterostructures and derive the transfer range x_0 experimentally, we have combined the one-dimensional exciton diffusion equation [Eq. (3.1)] for the photoexcitation density distribution $n(x,t)$ [14,30] with Eq. (5.6),

$$\frac{\partial n(x,t)}{\partial t} = D\frac{\partial^2 n(x,t)}{\partial x^2} - \frac{n(x,t)}{\tau_\infty}\left[1+\left(\frac{x_0}{x+d}\right)^3\right] + g(x,t). \tag{5.9}$$

The spatial variable x represents the distance from the polymer/spacer interface. In the second term, responsible for the decay of the exciton population, quenching by the metal is represented by a distance-dependent nonradiative energy-transfer subterm, where d stands for the thickness of the spacer layer. The last term describes the exciton generation process and is governed by the spatially dependent absorption profile of the femtosecond laser pulse. The contribution of interference effects into the photogeneration profile is negligible in view of the small thicknesses of the polymer films under consideration. Thus an exponential distance dependence of the intensity of the excitation beam reflected from the metal interface is used for $g(x,t)$. The time dependence of this term is approximated by a delta function, as the excitation pulse width (200 fs) is short in comparison to the dynamics of the quenching. At both polymer film interfaces the boundary condition $\partial n(x = L)/\partial x{=}0$ is applied, representing negligible surface quenching and the absence of exciton current on both boundaries. It should be noted that processing by spin coating implies that polymeric chains are mostly aligned in plane of the substrate. However, since exciton diffusion is mainly governed by interchain processes [31,32], in-plane exciton diffusion is expected not to prevail. Therefore, a one-dimensional model gives a good approximation of the exciton migration process.

In general, when the emissive layer is separated from the metal by a dielectric layer (Fig. 5.5), the expression for the transfer rate in Eq. (5.6) and the corresponding term in Eq. (5.9) have to be modified due to the difference in dielectric constants. If the spacer dielectric constant is larger than the dielectric constant of the emissive layer, it is expected that the energy-transfer rate to the metal becomes smaller because of the suppression of the electrostatic interaction of an oscillating dipole with the metal. In our study, the intermediate dielectric layer of LiF has a similar dielectric constant ($\varepsilon_\infty \approx 2$) as the emissive conjugated polymer [33,34]. Therefore, a direct substitution of Eq. (5.6) into the diffusion equation can be made, extending the distance x from the polymer/spacer interface with the spacer thickness d.

$$r_{me} = \frac{1}{\tau_\infty}\left(\frac{x_0}{x+d}\right)^3. \tag{5.10}$$

To account for the exciton lifetime τ_∞ the neat NRS-PPV film luminescence decay curve is recorded. A time-dependent exciton lifetime is used for analytical description of the nonmonoexponential luminescence decay [14]. Thus, the PL decay curve of the NRS-PPV/LiF/gold structure in Fig. 5.6 can now be numerically modeled by

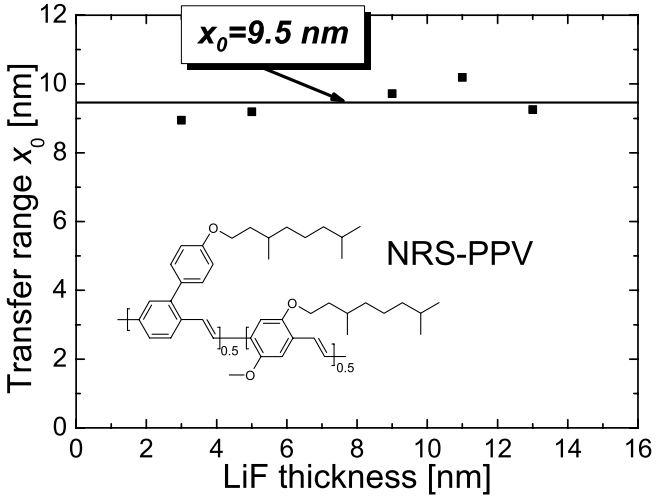

Figure 5.7: Energy-transfer range x_0 vs LiF spacer layer thickness in NRS-PPV/LiF/Au heterostructures. The inset shows the chemical structure of NRS-PPV.

Eq. (5.9), with the neat polymer luminescence decay as a reference. The only fit parameter, the energy-transfer range x_0, is derived to be 9.2 nm for NRS-PPV film in front of a gold mirror with a 5-nm LiF spacer in between. Thus, the process of the energy transfer to the metal is disentangled from the exciton migration mechanism, which in turn can be spatially characterized by the exciton diffusion length, $L_D \approx$ 6 nm in pristine NRS-PPV films [12, 14].

In order to verify the x^{-3} distance dependence in our system and check the assumption made in Eq. (5.10), we have varied the thickness of the LiF spacer layer. PL decay curves analogous to Fig. 5.6 as a function of polymer film thickness were recorded for LiF exciton blocking layers varying from 3 to 13 nm in thickness. Analysis of these data with Eq. (5.9) provided the energy-transfer range x_0 for polymer films at various distances from the quenching metal. When the distance dependence of the exciton quenching is correctly described by Eq. (5.10), the parameter x_0 should be independent on the geometry of the structure used. Indeed, as shown in Fig. 5.7, x_0 was found to be independent on the spacer layer thickness d within the range studied; x_0 only slightly fluctuates around an average number of 9.5 nm. This agreement proves the applicability of the inverse cubic distance dependence of the energy-transfer rate to the structures used in our study. Since the polymer film thickness is limited to only 35 nm, interference effects on the radiative lifetime can be excluded [3].

Present polymer LEDs and photovoltaic devices often employ a cathode that consists of a thin LiF layer with aluminum evaporated on top [35, 36]. Time-integrated PL quenching in NRS-PPV/LiF/Al heterostructures has been presented in Fig. 5.5. Subsequently, polymer luminescence decay curves were measured and, analogously to gold, analyzed in these structures for different thicknesses of a polymer film and

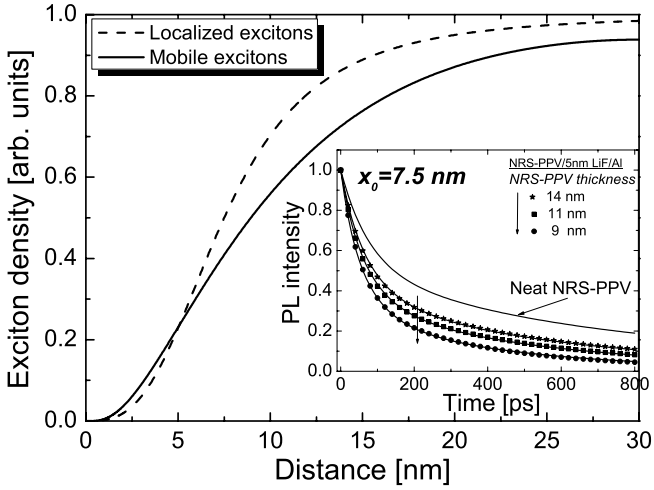

Figure 5.8: Steady-state exciton density profiles simulated for NRS-PPV/Al heterostructures with experimentally determined values for x_0 and D. The inset shows deconvoluted and normalized PL decay curves for NRS-PPV/LiF/Al structures for different polymer film thicknesses (symbols) with the simulation of these data by Eq. (5.9) with transfer range x_0=7.5 nm (solid lines).

constant thickness (5 nm) of the LiF spacer layer. In the inset of Fig. 5.8 luminescence decay curves are presented together with the fit to Eq. (5.9), which results in derivation of an energy-transfer range of 7.5 nm for the aluminum electrode. The reduction of the energy-transfer distance as compared to gold is predicted by theory (Eq. (5.7)) [7] and is in qualitative agreement with the higher imaginary part of the complex refractive index of aluminum ($K_2 = 6.33$) in comparison with gold ($K_2 = 2.86$) [37, 38].

With the energy-transfer range x_0 known we can simulate exciton density profiles at the polymer/Al interface, using x_0 and D as input parameters. In this simulation steady-state uniform exciton generation is assumed to demonstrate the effect of exciton quenching in terms of energy transfer and exciton diffusion. Figure 5.8 shows the redistribution of the steady-state exciton density profile due to exciton migration for NRS-PPV/LiF/Al heterostructures. Compared to "localized"excitons ($D = 0$) the exciton population is shifted further away from the metal interface due to the enhanced quenching. Furthermore, due to the diffusion-driven flow of excitons toward the metal interface, the exciton population at distances smaller than 5 nm exceeds the population of localized excitons. Relative quenching of mobile excitons estimated from areas under the curves in Fig. 5.8 for a 30-nm NRS-PPV film at an Al interface amounts to 38%, in contrast to 30% for virtually localized ones. Thus, the time-integrated relative quenching shown in Fig. 5.5 can now be quantitatively understood. The strong quenching, which is observed within a typical distance of

15 nm from the aluminum interface, is due to the direct energy transfer to the metal with a characteristic distance of 7.5 nm, being further enhanced by an exciton density redistribution characterized by a diffusion length of 6 nm.

5.4 Conclusions

In summary, we have studied exciton quenching in conjugated polymer films due to the presence of a metal contact. Time-resolved PL measurements have been performed for characterization of this process. Nonradiative energy transfer is disentangled from the exciton migration process by the use of a diffusion-assisted energy-transfer model. The inverse cubic distance dependence of the energy-transfer rate has been demonstrated to be applicable to polymer/metal structures at distances of several tens of nanometers. Analysis of the luminescence decay curves resulted in typical energy-transfer ranges of 9.5 and 7.5 nm for gold and aluminum, respectively.

Bibliography

[1] J. H. Burroughes, D. D. C. Bradley, A. R. Brown, R. N. Marks, K. Mackay, R. H. Friend, P. L. Burns, and A. B. Holmes, Nature (London) **347**, 539 (1990).

[2] N. C. Greenham, S. C. Moratti, D. D. C. Bradley, R. H. Friend, and A. B. Holmes, Nature (London) **365**, 628 (1993).

[3] H. Becker, S. E. Burns, and R. H. Friend, Phys. Rev. B **56**, 1893 (1997).

[4] N. S. Sariciftci, Prog. Quant. Electr. **19**, 131 (1995).

[5] C. J. Brabec, N. S. Sariciftci, and J. C. Hummelen, Adv. Funct. Mater. **11**, 15 (2001).

[6] P. Peumans, V. Bulovic, and S. R. Forrest, Appl. Phys. Lett. **76**, 2650 (2000).

[7] R. R. Chance, A. Prock, and R. Silbey, J. Chem. Phys. **62**, 2245 (1975).

[8] K. H. Drexhage, in *Progress in Optics*, edited by Wolf (North-Holland, Amsterdam, 1974), pp. 163-232.

[9] H. Kuhn, J. Chem. Phys. **53**, 101 (1970).

[10] P. Avouris and B. N. J. Persson, J. Phys. Chem. **88**, 837 (1984).

[11] R. R. Chance, A. H. Miller, A. Prock, and R. Silbey, J. Chem. Phys. **63**, 1589 (1975).

[12] D. E. Markov, E. Amsterdam, P. W. M. Blom, A. B. Sieval, and J. C. Hummelen, J. Phys. Chem. A **109**, 5266 (2005).

[13] J. J. M. Halls, K. Pichler, R. H. Friend, S. C. Moratti, and A. B. Holmes, Appl. Phys. Lett. **68**, 3120 (1996).

[14] D. E. Markov, J. C. Hummelen, P. W. M. Blom, and A. B. Sieval, Phys. Rev. B **72**, 045216 (2005).

[15] D. E. Markov, C. Tanase, P. W. M. Blom, and J. Wildeman, Phys. Rev. B **72**, 045217 (2005).

[16] A. Dodabalapur, L. J. Rothberg, R. H. Jordan, T. M. Miller, R. E. Slusher, and J. M. Phillips, J. Appl. Phys. **80**, 6954 (1996).

[17] J. R. Lakowicz, Analytical Biochemistry **298**, 1 (2001).

[18] S. E. Burns, N. Pfeffer, J. Grüner, M. Remmers, T. Javoreck, D. Neher, and R. H. Friend, Adv. Mater. **9**, 395 (1997).

[19] K. H. Drexhage, J. Luminescence **1,2**, 693 (1970).

[20] K. H. Drexhage, *Optische Untersuchungen an neuartigen monomolekularen Farbstoffschichten*, (Habititations-Schrift, Marburg, 1966).

[21] R. R. Chance, A. H. Miller, A. Prock, and R. Silbey, Chem. Phys. Lett. **33**, 590 (1975).

[22] G. Vaubel, H. Baessler, and D. Mobius, Chem. Phys. Lett. **10**, 334 (1971).

[23] A. Campion, A. R. Gallo, C. B. Harris, H. J. Robota, and P. M. Whitmore, Chem. Phys. Lett. **73**, 447 (1980).

[24] B. N. J. Persson and N. D. Lang, Phys. Rev. B **26**, 5409 (1982).

[25] G. Cnossen, K. E. Drabe, and D. A. Wiersma, J. Chem. Phys. **98**, 5276 (1993).

[26] K. G. Sullivan, O. King, C. Sigg, and D. G. Hall, Appl. Optics **33**, 2447 (1994).

[27] W. R. Holland and D. G. Hall, Phys. Rev. Lett. **52**, 1041 (1984).

[28] G. Vaubel, H. Baessler, and D. Mobius, Chem. Phys. Lett. **10**, 334 (1971).

[29] G. Cnossen, K. E. Drabe, and D. A. Wiersma, J. Chem. Phys. **98**, 5276 (1993).

[30] A. L. Burin and M. A. Ratner, J. Phys. Chem. A **104**, 4704 (2000).

[31] B. J. Schwartz, Annu. Rev. Phys. Chem. **54**, 141 (2003).

[32] T. Q. Nguyen, J. J. Wu, V. Doan, B. J. Schwartz, and S. H. Tolbert, Science **288**, 652 (2000).

[33] H. C. F. Martens, H. B. Brom, and P. W. M. Blom, Phys. Rev. B **60**, R8489 (1999).

[34] F. Bernardini and V. Fiorentini, Phys. Rev. B **58**, 15292 (1998).

[35] J. Yoon, J. J. Kim, T. W. Lee, and O. O. Park, Appl. Phys. Lett. **76**, 2152 (2000).

[36] V. D. Mihailetchi, L. J. A. Koster, P. W. M. Blom, Appl. Phys. Lett. **85**, 970 (2004).

[37] P. B. Johnson and R. W. Christy, Phys. Rev. B **6**, 4370 (1972).

[38] G. Hass and J. E. Waylonis, J. Opt. Soc. Am. **51**, 719 (1961).